Lithuanian Journal of Physics, Vol. **62**, No. 1, pp. 10–20 (2022)

INVESTIGATION OF A WIDELY-TUNABLE SUBNANOSECOND BBO-BASED OPTICAL PARAMETRIC AMPLIFIER

G. Stanionytė, V. Tamulienė, R. Grigonis, and J. Vengelis

Laser Research Center, Vilnius University, Saulėtekio 10, 10223 Vilnius, Lithuania
Email: julius.vengelis@ff.vu.lt

Received 17 January 2022; revised 21 February 2022; accepted 22 February 2022

We report an experimental realization of a subnanosecond optical parametric amplifier (OPA) system in a beta barium borate (BBO) crystal pumped by the third harmonic of a passively Q-switched Nd:YAG microlaser system and seeded by the continuum generated in a photonic crystal fibre (PCF). It yields broadband continuous signal wavelength tunability in the visible spectrum range from 470 to 660 nm and the idler wavelength from 768 to 1450 nm. Besides the experimental data, the numerical simulation results of the BBO optical parametric amplifier are presented. The maximum output power of the subnanosecond BBO OPA is limited by laser induced damage in the BBO crystal by the pump radiation and seed radiation spectral power density. We also notice and discuss the effect of seed radiation on BBO OPA output radiation characteristics. The numerical simulations qualitatively agree with the experimental data.

Keywords: nonlinear optics, optical parametric oscillators and amplifiers, subnanoseconds pulses, continuum seed, beta barium borate crystal

PACS: 42.65.-k, 42.65.Yj, 42.81.-i, 42.70.Mp

1. Introduction

A huge variety of lasers is known to have a vast range of applications in industry, medicine, science, etc [1]. However, the inherent wavelength tunability of lasers is an issue in some fields such as spectroscopy, sensing, nonlinear microscopy, etc., where widely-tunable laser radiation is required [2–7]. Therefore, optical parametric amplifiers (OPAs) [8–10] and optical parametric generators (OPGs) [11] are used as sources of tunable coherent radiation. Due to the significant progress in laser development and nonlinear optical materials growth these devices are now advanced and widely available in terms of spectral coverage, output power and pulse duration [8, 12, 13]. For pump pulses longer than 1 ns, travelling-wave OPGs or optical parametric oscillators (OPGs with a resonator) are used [14, 15], while in the case of femtosecond pump pulses synchronous pumping optical parametric oscillators (OPO) setups or OPAs are used [16–20]. For pulse durations of several or several tens of picoseconds, both synchronous pumping technique [21–23] or travelling wave configuration can be used [24, 25]. In this regard, a uniquely complicated temporal interval is the subnanosecond (100 ps – 1 ns) pulse duration range. The aforementioned synchronous pumping technique cannot be realized due to a very long resonator length requirement set by low repetition rate subnanosecond laser systems, while a simple travelling wave setup cannot be implemented due to the laser-induced damage threshold (LIDT), which in the case of subnanosecond pulses is usually lower than the parametric generation threshold. Thus, subnanosecond optical parametric devices are very difficult to implement. Subnanosecond optical parametric devices would be more compact, cheaper and more robust than expensive and complex femtosecond parametric optical parametric generators or amplifiers, especially when the intended application does not require femtosecond temporal resolution, but nanosecond resolution is insufficient. Examples of such applications are some cases in pump-probe spectroscopy, gas sensing and laser tattoo removal. Currently, only several subnanosecond OPGs and OPAs generating tunable pulses in the IR have been

demonstrated [26–29] together with one demonstration of subnanosecond OPO [30]. In all these cases, periodically-poled nonlinear media (such as periodically poled lithium niobate) were used and quasi-phase matching was implemented.

In this paper, we present, to the best of our knowledge, the first subnanosecond OPA system based on a beta barium borate (BBO) crystal generating widely-tunable radiation in the visible spectrum range from 470 to 660 nm. BBO is a very popular nonlinear crystal, which has a broad transparency range and higher LIDT compared to those of periodically poled crystals. Moreover, the angular wavelength tuning method used with BBO crystals allows for continuous wavelength tenability, which is usually not the case for the quasi phase-matching method used with periodically poled nonlinear crystals. The demonstrated OPA uses the continuum generated in a photonic crystal fibre as a seed source, which enables parametric generation in a travelling wave configuration.

2. Experimental setup

The experimental setup of the designed subnanosecond BBO OPA system is depicted in Fig. 1. The pump source for the OPA is a passively Q-switched Nd:YAG master oscillator power amplifier (MOPA) laser system manufactured by *Standa Ltd.* and generating subnanosecond pulses at 1 kHz repetition rate.

The Nd:YAG MOPA laser has two outputs: it is optimized for the third harmonic (λ = 355 nm – we will term it as TH) radiation at the first output, but also emits fundamental (λ = 1064 nm – we will term it as FH) and second (λ = 532 nm – we will term it as SH) harmonics at the second output. SH radiation was not used in the experiment, so it was directed into the beam dump BD.

The measured duration of TH pulses was ~500 ps (FWHM level) and for FH pulses it was ~400 ps (FWHM level), while the maximum pulse energy was 90 and 100 μJ, respectively. FH of the MOPA laser (λ = 1064 nm) was used as a pump to generate a continuum in a highly nonlinear polarization-maintaining photonic crystal fibre (PCF) which in turn was used as seed radiation for the BBO OPA system. The pump for continuum generation was focused into the PCF using a 0.65 numerical aperture and a 40× magnification microscope objective, which together with the input coupling end of PCF was mounted on a *Thorlabs* NanoMax 300D three-axis translation stage. A highly nonlinear polarization-maintaining solid-core PCF manufactured by *NKT Photonics* was used and its length was 1 m. The PCF core diameter was d = 5 μm which corresponded to a mode field diameter of 4.4 μm. A scanning electron microscope picture of this PCF cross-section is depicted in Fig. 2. Polarization

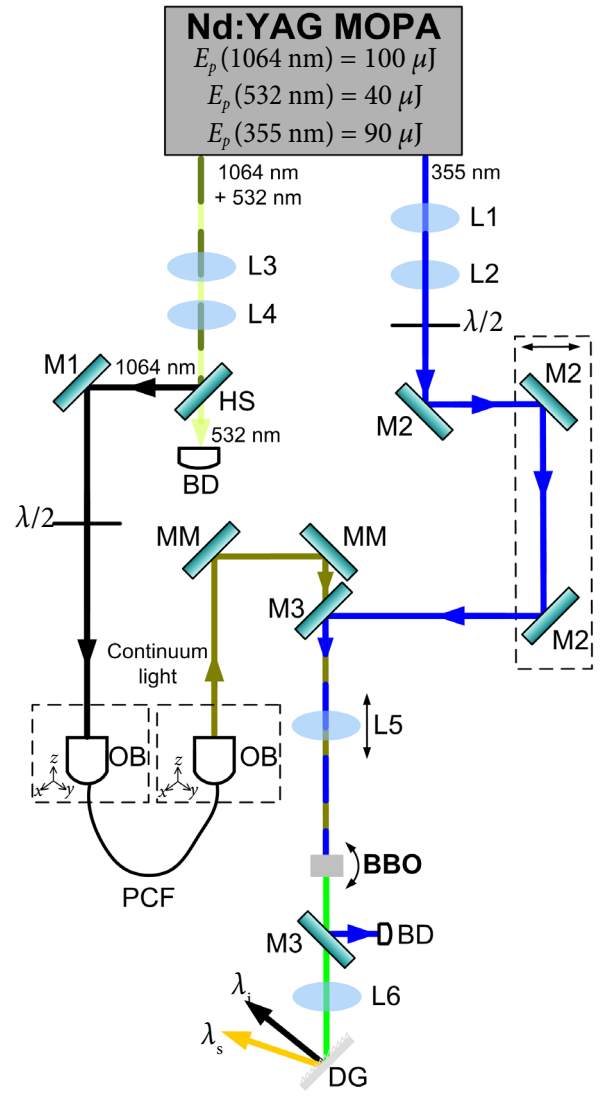

Fig. 1. The experimental setup: M1, highly reflective mirror for 1064 nm radiation; M2, highly reflective mirror for 35 nm radiation; M3, highly reflective for 355 nm and highly transmitting for 400–1500 nm radiation mirror; HS, harmonic separator mirror; MM, silver coated mirror; L1–L6, lenses; BD, beam dump; λ/2, half-wave plate; OB, 40× magnification microscope objective; PCF, highly nonlinear photonic crystal fibre; BBO, beta barium borate crystal; DG, diffraction grating.

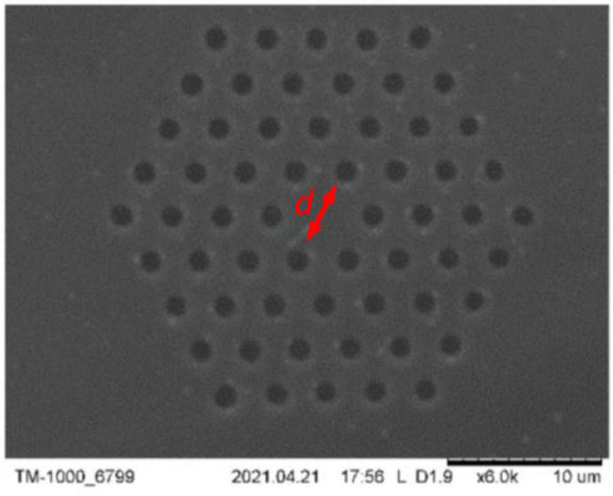

Fig. 2. The scanning electron microscope image of the PCF cross-section used for continuum generation.

is maintained by using stress inducing rods in the cladding, which are outside the microstructured region and therefore not visible in the image.

The generated continuum radiation and pump radiation were focused into a 6 mm (height) × 9 mm (width) × 15 mm (thickness) BBO crystal cut at $\theta = 28.2°$ and $\phi = 90°$ for type I phase matching using a 150 mm focal length lens L5. The BBO crystal was antireflection (AR)-coated for the λ = 355 nm and λ = 400–760 nm spectral range and mounted on a rotational stage to enable angular wavelength tuning. A delay line was used in the pump pulse line to achieve the maximum temporal overlap with seed pulses to maximize their nonlinear interaction. The generated signal and idler wave radiation was collimated using lens L6 and then the spatial separation of the signal and idler waves was performed with the use of a diffraction grating.

The continuum radiation generated in PCF was used as seed in our BBO OPA system. The seed spectrum at the maximum FH pump power is depicted in Fig. 3. Vertical polarization (with respect to PCF principal axes of polarization) FH radiation was used to pump PCF because the generated continuum spectra in this case were slightly broader. It is important to note that the LIDT of the PCF material (fused silica) limited the maximum pump power that we could use for continuum generation. The maximum used continuum pump power was 7.5 mW, which was roughly 75% of the LIDT power of the PCF material, and yielded roughly 5.7 mW seed power in the output (throughout the entire seed spectrum). At the maximum FH pump power the continuum spectrum extended approximately from 720 to 1600 nm. The maximum OPA TH pump power was limited by LIDT of the BBO crystal, thus the maximum pump power that we used was 23 mW.

The principle of our subnanosecond BBO OPA system operation is as follows. The generated continuum radiation is seed for the parametric amplification of the longer wavelength (idler) wave. The difference frequency wave generated in the process has a shorter wavelength than the seed radiation, thus we call it the signal wave. In this case, the signal wave covers the visible spectrum range – the spectrum region that was aimed for the BBO OPA operation.

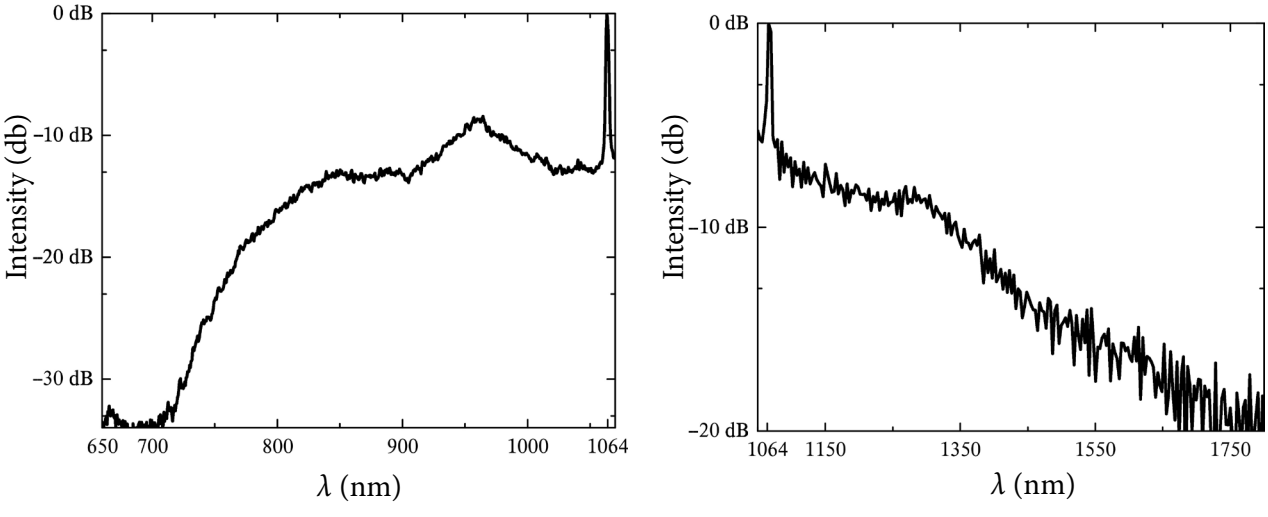

Fig. 3. The generated continuum spectrum at the maximum FH pump power (P = 7.5 mW). Spectra were measured using two separate spectrometers that cover different spectral ranges.

3. Experimental results

The achieved signal wave tuning range was from 470 to 660 nm and corresponded to the BBO crystal angular tuning range from 28.7 to 31.3° (Fig. 4, right). Since the theoretical signal wave tuning range in the BBO crystal at 355 nm pump should be from 396 to 710 nm, practical limitation of the tuning range was essentially set by the seed spectrum extent: the 470 nm signal wavelength corresponds to the 1450 nm idler wavelength, which is close to the seed (continuum) spectral edge, and the 660 nm signal wavelength corresponds to the 768 nm idler wavelength, which is also close to the seed radiation spectral edge. The seed spectrum can be extended by using a longer PCF, but in such case losses in the longer PCF would be greater and we would have less seed power, therefore we chose a greater seed power over a slightly broader signal wave tuning range.

Although the bandwidth of 500 ps duration pump pulses is estimated to be roughly $\Delta\lambda = 0.37$ pm, generated signal wave spectral bandwidths (at FWHM level) are of the order of nanometres and in a range from 0.6 to 13 nm. This indicates that the generated signal wave pulses have a significant chirp. At longer wavelengths (such as 625 nm wavelength, with spectrum depicted in Fig. 4, left), the signal spectra are even broader since they approach the degenerate regime.

Energy characteristics of the BBO OPA were measured at the maximum seed power (P_{seed} = 5.7 mW) and the FH pump polarization was set to correspond to the maximum spectral extent of the seed (continuum) spectrum. The maximum signal wave power at different wavelengths is depicted in Fig. 5 (left). The first important thing to note is that the pump to signal conversion efficiency is very low and does not exceed 0.35% for any wavelength. Such result is related to very complicated subnanosecond BBO OPA operation conditions: a low spectral power density of the seed radiation, a low pump intensity and a relatively large spatial walk-off effect in the BBO crystal. The nonlinear interaction length for the signal wave in theory should be around 14 mm; however, due to the spatial walk-off effect between pump and signal, the actual interaction length at our focusing conditions was 3–4 mm (depending on the signal wavelength). The 5.7 mW seed power is the overall power through the entire continuum spectrum, but the spectral power density for distinct wavelengths varies by several orders of magnitude (Fig. 3), e.g. at 1168 nm seed wavelength (which corresponds to 510 nm signal wavelength) the spectral power density is only 210 nW/nm.

The low pump power problem is related to the fact that the maximum peak intensity of the TH pump is roughly 1.45 GW/cm^2 which is relatively low and sharper focusing conditions cannot be used due to the LIDT of the BBO crystal. Another important factor regarding the BBO crystal is the spatial walk-off effect between pump and signal waves which ranges from 69 to 74 mrad across

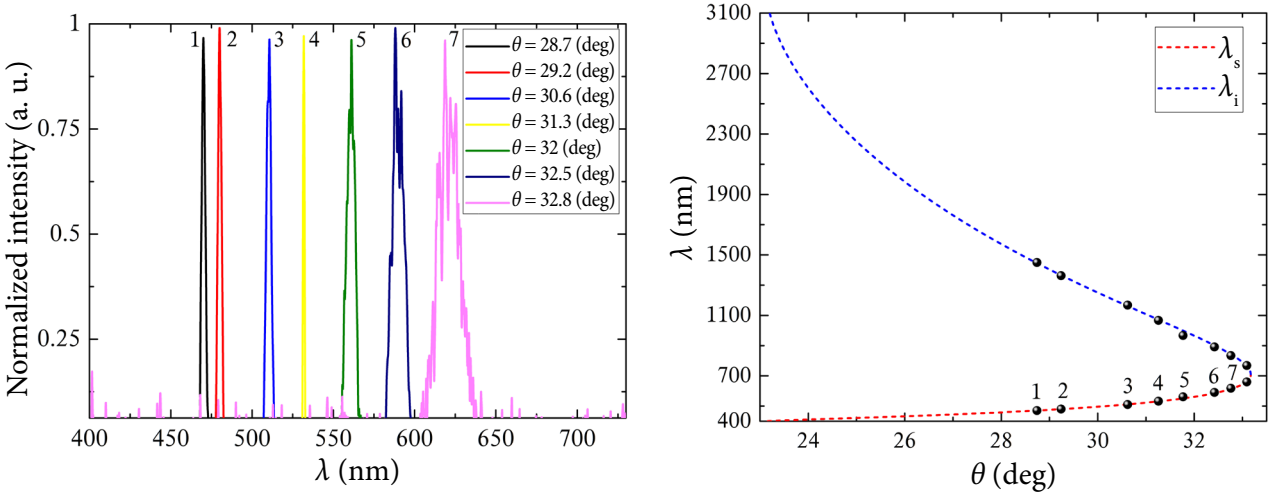

Fig. 4. The measured signal wave spectra at different BBO crystal rotation angles (left); the BBO crystal angular tuning curve when λ_p = 355 nm (BBO): dots indicate experimentally measured values, dashed lines show theoretically calculated values, while numbers next above the experimental data points correspond to the measured spectra in the left picture.

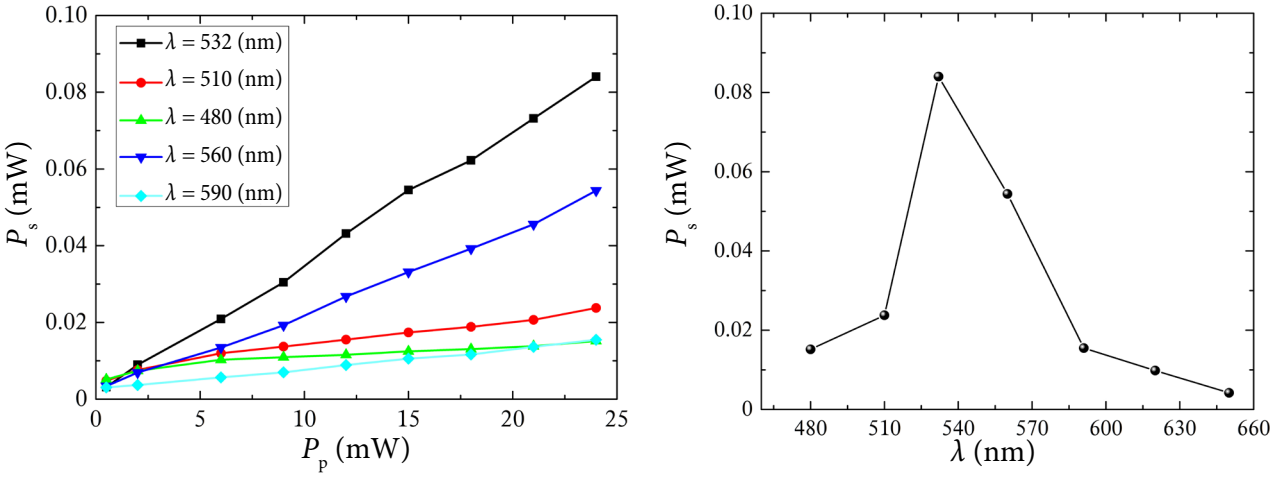

Fig. 5. The measured BBO OPA signal wave output power dependence on TH pump power (left) when seed power is maximum (P_{seed} = 5.7 mW); the measured BBO OPA maximum signal output power dependence on the wavelength at the maximum seed power (right).

the signal wave tuning range. Such walk-off values even at the current soft focusing conditions limit the nonlinear interaction length in the BBO crystal.

The second important feature, which is also visible from the signal wave power dependence on pump power (Fig. 5, left), is a considerably greater power of the λ = 532 nm signal wave. This is related to the aforementioned seed radiation spectral power density variations: seed (continuum) generation efficiency is low and most of the energy remains concentrated at the seed (continuum) pump wavelength (1064 nm), which corresponds to 532 nm signal wavelength.

The seed radiaton influence to signal wave power was further investigated by measuring the signal wave power dependence on seed power, with the pump power fixed at the maximum value (P_{TH} = 23 mW). Seed power was adjusted by changing the seed pump (FH) power, which also considerably changed the spectral characteristics of the seed radiation. Results for most wavelengths are very similar to the signal wave maximum power dependence on the pump pulse power depicted in Fig. 5 (left); however, for the signal wavelength around 532 nm the dependence is different (Fig. 6(a)).

When seed radiation power is decreased, an increase of signal wave power up to 0.264 mW, which corresponds to 1.15% pump to signal conversion efficiency, is observed. It peaks at P_{seed} = 2 mW and then signal wave power starts to decrease. This effect and its occurrence for λ_s = 532 nm can be explained as follows. Decreasing seed pump power reduces the continuum spectral extent (Fig. 6(b, c)), but raises the spectral power density of the pump FH wavelength, which corresponds to the λ = 532 nm signal wavelength, and thus compensates the decrease of spectral intensity due to decreasing seed pump power. Therefore, an increase of power is observed for the λ = 532 nm signal wavelength, but is negligible for other wavelengths where no noticeable spectral intensity increase due to the shrinking continuum spectrum was observed. When seed power is decreased below 2 mW, the seed spectrum width is reduced to the vicinity of the seed pump wavelength (1064 nm) and the further spectral intensity increase due to the shrinking continuum bandwidth does not exceed the intensity loss due to decreasing pump power, resulting in decreasing signal wave at λ = 532 nm power.

Another important characteristic that was measured is the signal pulse duration. We used the time-correlated single photon counting (TCSPC, [31]) system PicoHarp 300 to estimate the duration of BBO OPA signal wave pulses. The TCSPC system measures signal photon arrival time statistics with respect to a reference signal, which in this case was an optical signal: a reference photodiode was used to provide an optical signal from SH pulses generated by our Nd:YAG MOPA laser system. The retrieved signal photon arrival time histogram was approximated by a Gaussian function and pulse duration was estimated at the FWHM level (Fig. 7, left). The temporal resolution of our TCSPC measurement setup was 16 ps.

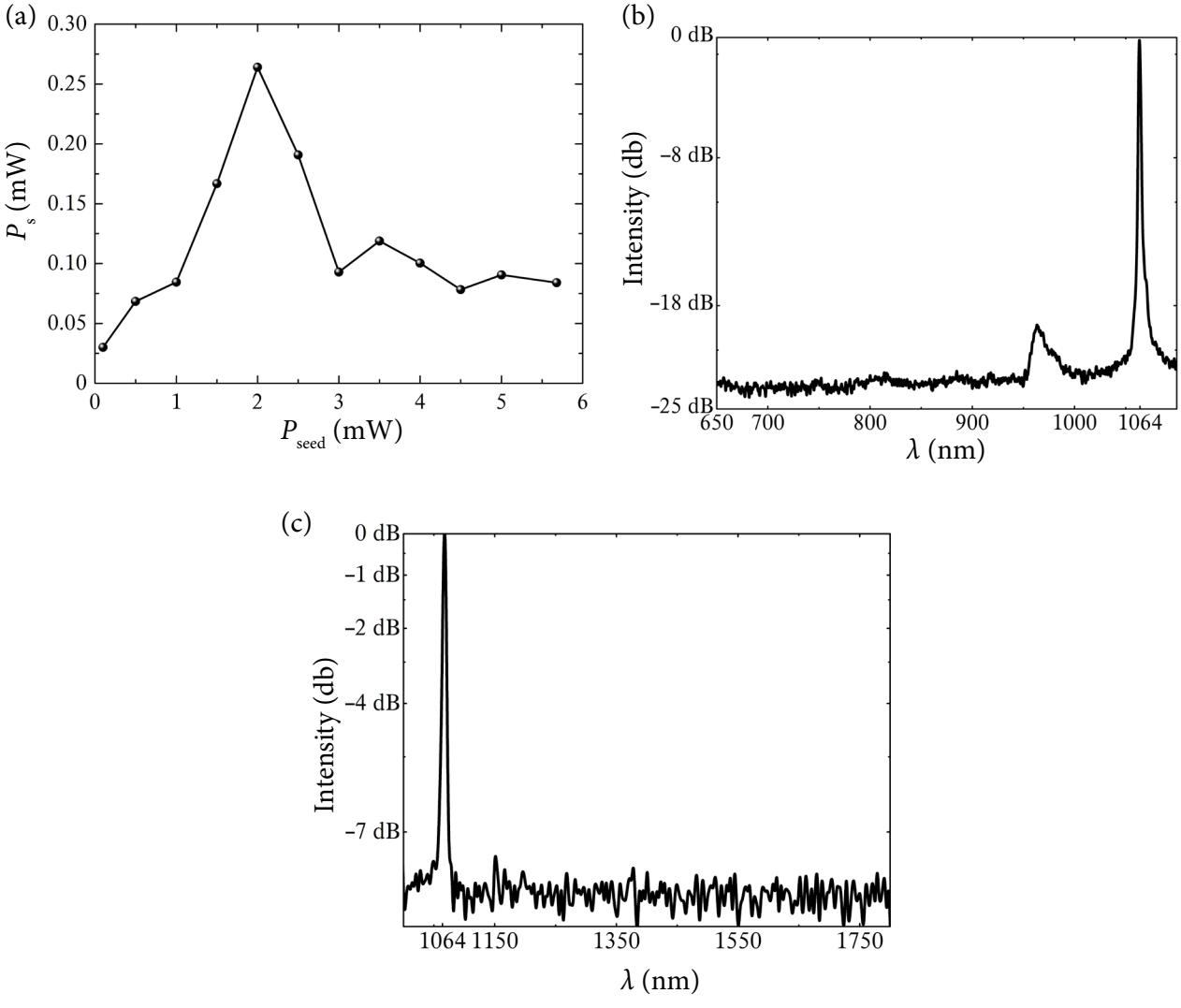

Fig. 6. (a) the measured BBO OPA signal wave at the λ = 532 nm maximum output power dependence on seed power; (b) the measured NIR part of the seed radiation spectrum at P_{FH} = 2 mW; (c) the measured IR part of the seed radiation spectrum at P_{FH} = 2 mW.

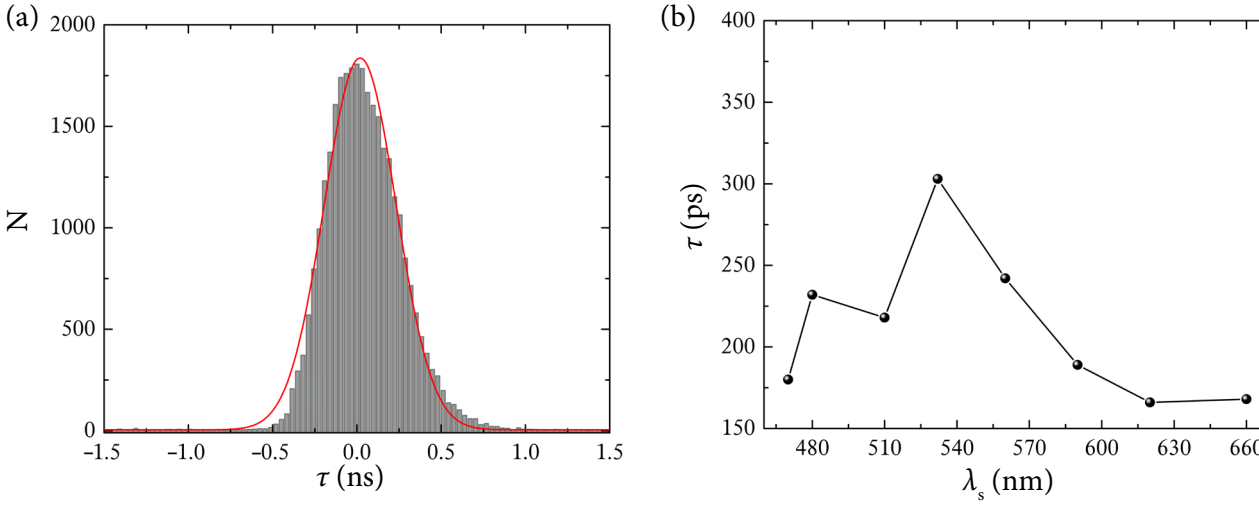

Fig. 7. The measured TH pump pulse TCSPC histogram (left) with the corresponding Gaussian function fit (red curve); the measured BBO OPA signal pulse duration (right) at various wavelengths.

The measured signal pulse durations are depicted in Fig. 7 (right). The generated signal pulses have subnanosecond durations ranging from 166 to 303 ps. Longer generated pulse duration correlates with a greater maximum output power, indicating that stronger nonlinear interaction yields signal pulse duration closer to the pump pulse (500 ps) duration.

Signal pulse duration essentially remains the same (within the 16 ps temporal resolution limit of the TCSPC setup) when changing the pump power (Fig. 8, left), which is the case when parametric amplification has a low efficiency and is far from the pump depletion regime. However, seed radiation and its temporal matching with pump radiation significantly affects the generated signal pulse duration (Fig. 8, right).

The exact temporal matching (zero delay) corresponds to the maximum output power and the minimum generated pulse duration. When there is a certain delay between pump and seed radiation, generated signal pulses have lower power and longer duration. This effect is due to the fact that seed radiation (continuum) obeys the complex temporal characteristic, which is longer (>1 ns) than that of the pump pulse. When pump pulses are delayed with respect to seed radiation, the temporal peak of seed radiation does not match the peak of pump pulses and the energy of seed and pump radiation is redistributed in a broader time interval – the generated signal wave duration increases.

4. Results of numerical simulation and discussion

We have performed the numerical simulations of the three-wave nonlinear interaction equations including the dispersion terms:

$$\frac{\partial S_1}{\partial z} = \mathrm{i}K_1 S_1 + \sigma_1 FT[A_2^* A_3], \tag{1}$$

$$\frac{\partial S_2}{\partial z} = \mathrm{i}K_2 S_2 + \sigma_2 FT[A_1^* A_3], \tag{2}$$

$$\frac{\partial S_3}{\partial z} = \mathrm{i}K_3 S_3 - \sigma_3 FT[A_1 A_2]. \tag{3}$$

Here, $S_j(\Omega)$ is the Fourier transform of the complex amplitude $A_j(t)$ and the real electric field is given by $E(t, z) = \Re[A(t, z)\exp^{(\mathrm{i}\omega_{j0}t)}]$. Indices 1, 2 and 3 refer to the signal, idler and pump waves, respectively. The first rhs terms describe the linear dispersion. $K_j(\omega) = k_j(\omega_j) - \frac{\Omega}{u_{30}}$ is the wavenumber (k_j) shifted with respect to the pump wave propagation. ω is the radial frequency and u_{30} is the pump group velocity. The nonlinear interaction coefficient is $\sigma_j = d_{\mathrm{eff}}\omega_{j0}/(cn_j(\lambda_{j0}))$. Here d_{eff} is the effective nonlinear susceptibility that depends on the crystal orientation [32], c is the speed of light and n_j is the refractive index at the central wavelength λ_{j0} calculated from the Sellmeier equations for the BBO crystal [32]. *FT* [◦] denotes the Fourier transform. Eqs. (1–3) were simulated by the symmetrized split-step

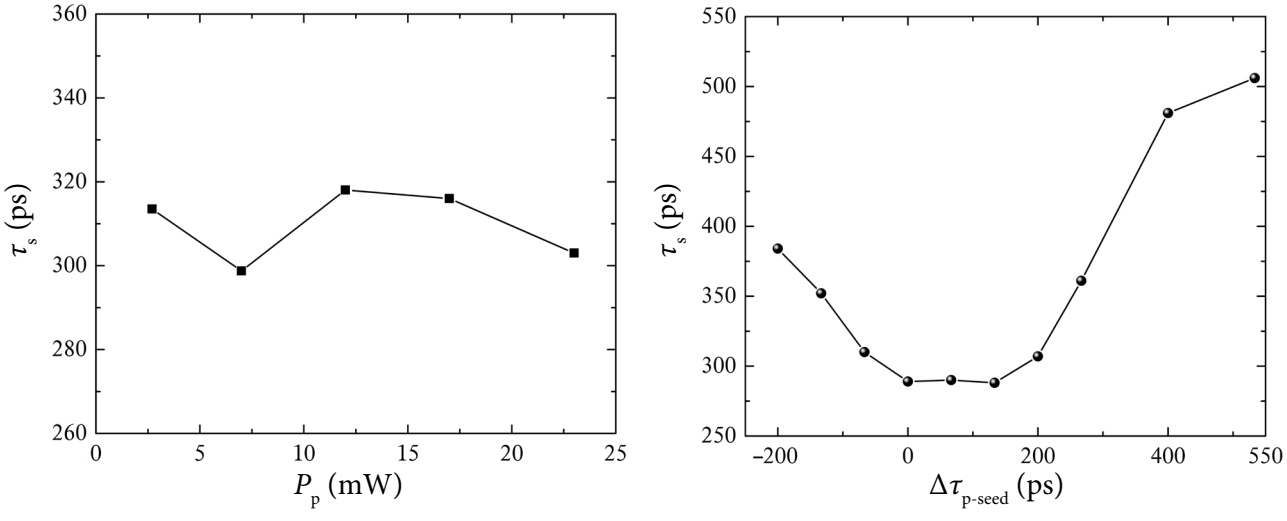

Fig. 8. The measured λ = 532 nm signal pulse duration at various TH pump powers (left); the measured λ = 532 nm signal pulse duration dependence on the temporal delay between TH pump and seed radiation (right). Negative delay values mean that TH pump pulses are ahead of the seed radiation.

Fourier method [33]. The crystal length L = 15 mm was divided into 500 longitudinal steps. The boundary condition for the pump wave can be expressed as

$$A_3(t, z=0) = a_{30} \exp\left(-2 \ln 2 \frac{t^2}{\tau^2}\right). \quad (4)$$

Here a_{30} is the input amplitude and τ = 500 ps is the pulse duration at FWHM. The pump wave is the Gaussian subnanosecond pulse. There was no signal wave at the input, $A_1(t, z = 0) = 0$. The input idler wave was simulated from the experimentally measured spectrum. The spectra displayed in Fig. 3 were combined and linearly interpolated so that in the time domain they were subdivided into 2^{22} equal steps. The time interval was $[-16\tau, 16\tau)$. Afterwards, 1/16 part of the spectrum was cut from the spectrum at the predefined central frequency (for example, frequency corresponding to 1064 nm wavelength). This part of the spectrum was multiplied by the chirp phase factor: $\exp(i\gamma\Omega^2\tau^2)$, where the non-dimensional chirp parameter $\gamma = 10^{-4}$. Such chirp expands the idler time pulse to several nanoseconds. In the simulations, the input pump power was 23 mW, the repetition rate 1 kHz and the beam diameter 1.5 mm. The input idler power was 5 mW.

The numerically obtained results are presented in Fig. 9. Five spectra in Fig. 9(a) correspond to a different phase matching (type I) angles BBO crystal. As in the experiment, the maximum output power is obtained at 532 nm wavelength that corresponds to the idler peak at 1064 nm. The curve in Fig. 9(b) resembles the experimental data: numerically simulated signal wave power is low (fractions of miliwatts), similar to Fig. 5(b). However, the output power is higher than the measured one since the spatial effects like diffraction and walk-off between ordinary and extraordinary waves were neglected in the numerical simulation.

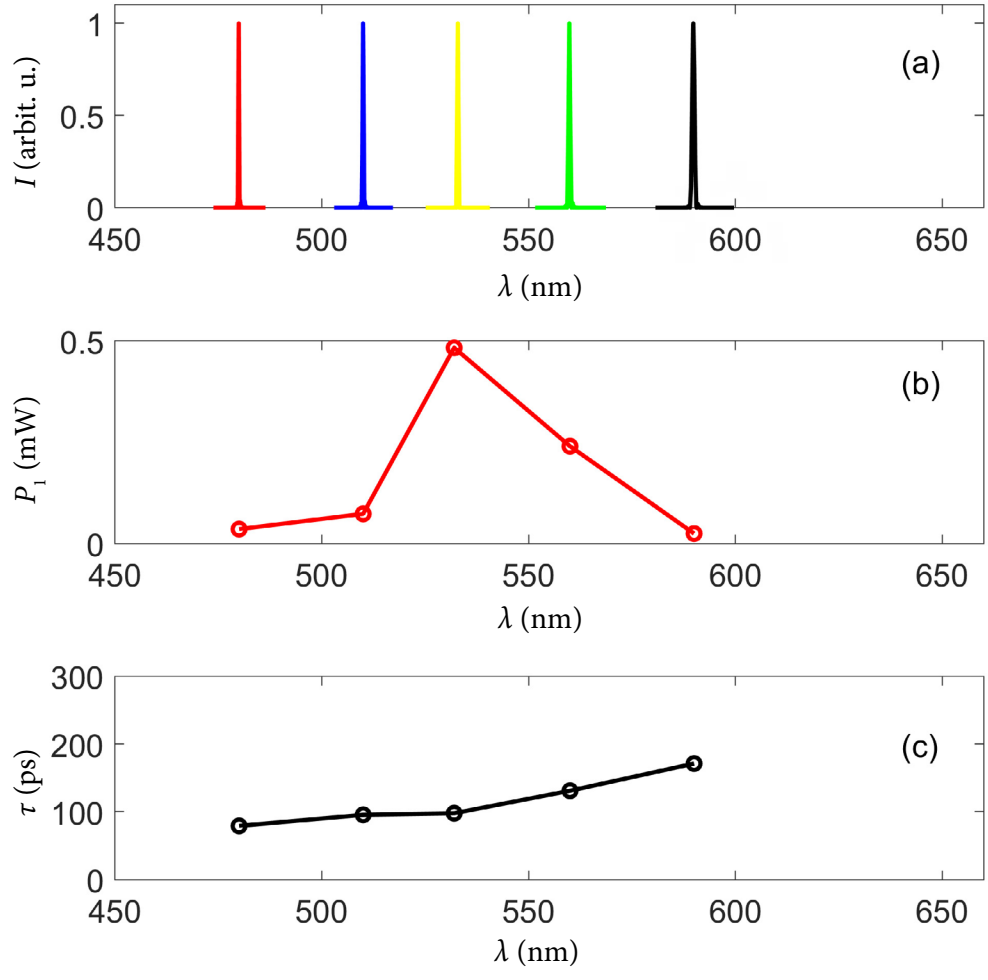

Fig. 9. Numerical simulation results. Signal output spectra (a), power (b) and pulse duration at FWHM (c).

The pulse duration in Fig. 9(c) does not coincide exactly with the experimental duration (Fig. 7) due to the chirp parameter that in the numerical simulations was equal for all spectral parts. The real continuum spectrum obeys a complicated spectral phase that could not be measured. However, the numerically calculated pulse profiles qualitatively agreed with the experiment – signal pulses were in the subnanosecond range.

5. Conclusions

To the best of our knowledge, the first widely-tunable in the visible spectrum range BBO optical parametric amplifier generating subnanosecond pulses was demonstrated and its spectral energy and temporal characteristics were investigated. The continuous signal wavelength tuning in the 470–660 nm spectral range was achieved and was limited by the seed radiation spectral extent. The maximum pump to signal conversion efficiency was low (1.15%) due to a strong spatial walk-off effect in the BBO crystal and the limitation of the maximum pump power due to the laser induced damage threshold in the BBO by the pump pulses. Seed radiation spectral energy distribution was the key factor determining that the maximum signal wave power was at λ = 532 nm, which corresponded to the 1064 nm idler wavelength for which seed spectral power density was the highest. This indicates that a greater pump to signal coversion efficiency could be achieved with a more powerful seed source and additional parametric amplification stages. The pulse duration measurements showed that the generated pulses also have subnanosecond durations ranging from 166 to 303 ps at different signal wavelengths. The numerical simulations displayed qualitatively similar results and slight discrepancies were related to some factors not accounted for in them.

Acknowledgements

This work has received funding from the European Regional Development Fund (Project No. 01.2.2-LMT-K-718-03-0004) under Grant Agreement with the Research Council of Lithuania. We also thank Prof. Mikas Vengris for his advice and technical assistance during TCSPC measurements.

References

[1] K. Thyagarajan and A. Ghatak, *Lasers: Fundamentals and Applications* (Springer Science & Business Media, London, 2010).

[2] J.G. Haub, M.J. Johnson, and B.J. Orr, Spectroscopic and nonlinear-optical applications of a tunable β-barium borate optical parametric oscillator, J. Opt. Soc. Am. B **10**(9), 1765–1777 (1993).

[3] D.D. Arslanov, M.P. Castro, N.A. Creemers, A.H. Neerincx, M. Spunei, J. Mandon, S.M. Cristescu, P.J. Merkus, and F.J. Harren, Optical parametric oscillator-based photoacoustic detection of hydrogen cyanide for biomedical applications, J. Biomed. Opt. **18**(10), 1–9 (2013).

[4] K. Fradkin-Kashi, A. Arie, P. Urenski, and G. Rosenman, Mid-infrared difference–frequency generation in periodically poled $KTiOAsO_4$ and application to gas sensing, Opt. Lett. **25**(10), 743 (2000).

[5] S. Cussat-Blanc, A. Ivanov, D. Lupinski, and E. Freysz, $KTiOPO_4$, $KTiOAsO_4$, and $KNbO_3$ crystals for mid-infrared femtosecond optical parametric amplifiers: Analysis and comparison, Appl. Phys. B **70**(Suppl. 1), 247–252 (2000).

[6] K.A. Tillman, R.R. Maier, D.T. Reid, and E.D. McNaghten, Mid-infrared absorption spectroscopy of methane using a broadband femtosecond optical parametric oscillator based on aperiodically poled lithium niobate, J. Opt. A Pure Appl. Opt. **7**(6), S408–S414 (2005).

[7] V. Andresen, S. Alexander, W.M. Heupel, M. Hirschberg, R.M. Hoffman, and P. Friedl, Infrared multiphoton microscopy: subcellular-resolved deep tissue imaging, Curr. Opin. Biotechnol. **20**(1), 54–62 (2009).

[8] M.H. Dunn and M. Ebrahimzadeh, Parametric generation of tunable light from continuous-wave to femtosecond pulses, Science **286**(5444), 1513–1517 (1999).

[9] G. Cerullo and S. De Silvestri, Ultrafast optical parametric amplifiers, Rev. Sci. Instrum. **74**(1 I), 1–18 (2003).

[10] D. Brida, C. Manzoni, G. Cirmi, M. Marangoni, S. Bonora, P. Villoresi, S. De Silvestri, and G. Cerullo, Few-optical-cycle pulses tunable from

the visible to the mid-infrared by optical parametric amplifiers, J. Opt. A Pure Appl. Opt. **12**(1), 013001 (2010).

[11] M. Ebrahimzadeh, Parametric light generation, Philos. Trans. R. Soc. A **361**(1813), 2731–2750 (2003).

[12] D.T. Reid, C.M. Heyl, R.R. Thomson, R. Trebino, G. Steinmeyer, H.H. Fielding, R. Holzwarth, Z. Zhang, P. Del'Haye, T. Südmeyer, G. Mourou, T. Tajima, D. Faccio, F.J. Harren, and G. Cerullo, Roadmap on ultrafast optics, J. Opt. **18**(9), 1–32 (2016).

[13] M. Ebrahim-Zadeh, S.C. Kumar, A. Esteban-Martin, and G.K. Samanta, Breakthroughs in photonics 2012: Breakthroughs in optical parametric oscillators, IEEE Photonics J. **5**(2), 10–15 (2013).

[14] U. Bäder, J.-P. Meyn, J. Bartschke, T. Weber, A. Borsutzky, R. Wallenstein, R.G. Batchko, M.M. Fejer, and R.L. Byer, Nanosecond periodically poled lithium niobate optical parametric generator pumped at 532 nm by a single-frequency passively Q-switched Nd:YAG laser, Opt. Lett. **24**(22), 1608 (1999).

[15] M.S. Webb, P.F. Moulton, J.J. Kasinski, R.L. Burnham, G. Loiacono, and R. Stolzenberger, High-average-power $KTiOAsO_4$ optical parametric oscillator, Opt. Lett. **23**(15), 1161 (1998).

[16] I. Pipinytė, V. Tamulienė, J. Vengelis, R. Grigonis, and V. Sirutkaitis, Temporal characteristics of a synchronously pumped optical parametric oscillator at different conditions of cavity losses, J. Opt. Soc. Am. B **36**(10), 2735 (2019).

[17] F. Ruebel, G. Anstett, and J.A. L'huillier, Synchronously pumped mid-infrared optical parametric oscillator with an output power exceeding 1 W at 4.5 μm, Appl. Phys. B **102**(4), 751–755 (2011).

[18] B. Teng, S. Dong, Y. Ding, Z. Wang, J. Wang, R. Mao, Z. Zhai, Z. Yu, X. Sun, and P. Ma, BiB_3O_6 nanosecond optical parametric oscillator, Opt. Lett. **28**(10), 1998–2001 (2008).

[19] J. Vengelis, I. Stasevičius, K. Stankevičiutė, V. Jarutis, R. Grigonis, M. Vengris, and V. Sirutkaitis, Characteristics of optical parametric oscillators synchronously pumped by second harmonic of femtosecond Yb:KGW laser, Opt. Commun. **338** (2015).

[20] Y. Stepanenko and C. Radzewicz, Multipass noncollinear optical parametric amplifier for femtosecond pulses, Opt. Express **14**(2), 779 (2006).

[21] L.J. Bromley, A. Guy, and D.C. Hanna, Synchronously pumped optical parametric oscillation in beta-barium borate, Opt. Commun. **67**, 316–320 (1988).

[22] L. Lefort, K. Puech, S.D. Butterworth, G.W. Ross, P.G. Smith, D.C. Hanna, and D.H. Jundt, Efficient, low-threshold synchronously-pumped parametric oscillation in periodically-poled lithium niobate over the 1.3 μm to 5.3 μm range, Opt. Commun. **152**(1–3), 55–58 (1998).

[23] B. Ruffing, A. Nebel, and R. Wallenstein, High-power picosecond LiB_3O_5 optical parametric oscillators tunable in the blue spectral range, Appl. Phys. B **72**(2), 137–149 (2001).

[24] J.Y. Huang, J.Y. Zhang, and Y.R. Shen, High-power, widely tunable, picosecond coherent source from optical parametric amplification in barium borate, Appl. Phys. Lett. **57**(19), 1961–1963 (1990).

[25] J.Y. Zhang, J.Y. Huang, Y.R. Shen, C. Chen, and B. Wu, Picosecond optical parametric amplification in lithium triborate, Appl. Phys. Lett. **58**(3), 213–215 (1991).

[26] M.D. Cocuzzi, K.L. Schepler, and P.E. Powers, Narrow-bandwidth, subnanosecond, infrared pulse generation in PPLN pumped by a fiber amplifier-microchip oscillator, IEEE J. Sel. Top. Quant. Electron. **15**(2), 372–376 (2009).

[27] H. Ishizuki and T. Taira, in: *Advanced Solid State Lasers, ASSL 2015* (2015), 4–6.

[28] L. Liu, H.Y. Wang, Y. Ning, C. Shen, L. Si, Y. Yang, Q.L. Bao, and G. Ren, Sub-nanosecond periodically poled lithium niobate optical parametric generator and amplifier pumped by an actively Q-switched diode-pumped Nd:YAG microlaser, Laser Phys. **27**(5), 055403 (2017).

[29] J.-P. Fève, B. Boulanger, B. Ménaert, and O. Pacaud, Continuous tuning of a microlaser-pumped optical parametric generator by use of a cylindrical periodically poled lithium niobate crystal, Opt. Lett. **28**(12), 1028 (2003).

[30] G. Marchev, P. Dallocchio, F. Pirzio, A. Agnesi, G. Reali, V. Petrov, A. Tyazhev, V. Pasiskevicius, N. Thilmann, and F. Laurell, Sub-nanosecond, 1–10 kHz, low-threshold, noncritical OPOs based on periodically poled KTP crystal pumped at 1,064 nm, Appl. Phys. B **109**(2), 211–214 (2012).

[31] D.V. O'Connor and D. Phillips, *Time-correlated Single Photon Counting* (Academic Press, Orlando, 1984).

[32] D.N. Nikogosyan, *Nonlinear Optical Crystals: A Complete Survey* (Springer, Ireland, 2005).

[33] M.S. Wartak, *Computational Photonics: An Introduction with MATLAB* (Cambridge University Press, United Kingdom, 2013).

SUBNANOSEKUNDINIO PLAČIOJE SPEKTRO SRITYJE DERINAMO BBO OPTINIO PARAMETRINIO STIPRINTUVO TYRIMAS

G. Stanionytė, V. Tamulienė, R. Grigonis, J. Vengelis

Vilniaus universiteto Lazerinių tyrimų centras, Vilnius, Lietuva

Santrauka

Taikymuose, reikalaujančiuose tolygiai derinamo dažnio lazerinės spinduliuotės, naudojami parametriniai šviesos generatoriai ir stiprintuvai. Didelis tokių prietaisų poreikis lėmė spartų su jais susijusių technologijų tobulėjimą ir pritaikymą veikti kaupinant tiek nuolatinės veikos, tiek įvairių trukmių lazerio spinduliuote. Vis dėlto subnanosekundinių trukmių (100 ps – 1 ns) intervale parametrinių šviesos generatorių ir stiprintuvų realizavimas yra labai komplikuotas dėl subnanosekundinių trukmių intervale santykinai žemo lazerio indukuotos pažaidos slenksčio daugelyje medžiagų. Šiame darbe pristatomas, autorių žiniomis, pirmasis subnanosekundinis plačioje spektro srityje derinamas optinis parametrinis šviesos stiprintuvas, kai netiesinėje terpėje naudojamas beta bario borato (BBO) kristalas. Signalinės bangos ilgio derinimo sritis siekė 470–660 nm ir iš esmės buvo apribota užkrato spinduliuotės spektro pločio. Užkratu parametriniam stiprinimui pasirinkta kontinuumo spinduliuotė generuota fotoninių kristalų šviesolaidyje. Nustatyta, kad ne tik spektrinės, bet ir energinės užkrato charakteristikos iš esmės lemia generuotos spinduliuotės savybes. Maksimalus parametrinio keitimo efektyvumas iš kaupinimo į signalinę bangą buvo labai nedidelis (1,15 %) dėl erdvinio nunešimo efekto BBO kristale ir lazerio indukuotos pažaidos lemiamo kaupinimo spinduliuotės intensyvumo apribojimo. Jį padidinti būtų galima naudojant didesnio intensyvumo užkrato spinduliuotę arba papildomas parametrinio stiprinimo pakopas. Signalinės bangos trukmės skirtingiems signalinės bangos ilgiams taip pat buvo subnanosekundinių trukmių intervale (168–303 ps). Skaitinio modeliavimo rezultatai kokybiškai atitiko eksperimentinius duomenis.